Advanced Mobility Testbed for Dynamic Semi-Autonomous Unmanned Ground Vehicles

Paramsothy Jayakumar[†], **Abhinandan Jain**[*], **James Poplawski**[†], **Marco Quadrelli**[*], **Jonathan Cameron**[*], **Joseph Raymond**[†]

[†]U.S. Army TARDEC, 6501 E 11 Mile Rd, Warren, MI 48397, USA

[*]Jet Propulsion Laboratory, California Institute of Technology, 4800 Oak Grove Drive, Pasadena, California 91016, USA

1 Introduction

Integrated simulation capabilities that are high-fidelity, fast, and have scalable architecture are essential to support autonomous vehicle design and performance assessment for the U.S. Army's growing use of unmanned ground vehicles (UGVs). With increased onboard autonomy, advanced vehicle models are needed to analyze and optimize control design and sensor packages over a range of urban and off-road scenarios. Recent work at US Army TARDEC has attempted to develop a high-fidelity mobility simulation of an autonomous vehicle in an off-road scenario using integrated sensor, controller, and multi-body dynamics models [1]. The conclusion was that (a) real-time simulation was not feasible due to the complexity of the intervening formulation, (b) models had to be simplified to speed up the simulation, (c) interfacing the sensors was exceedingly difficult due to co-simulation, (d) the controls developed were very basic and could not be optimized, and (e) a rigid terrain model was used.

The research described in this paper is from a collaborative project between US Army TARDEC and NASA Jet Propulsion Laboratory (JPL) to develop an advanced UGV mobility testbed using JPL's ROAMS vehicle modeling capability [2] and to address the aforementioned issues in meeting the US Army's UGV modeling and simulation needs. The ROAMS ground vehicle simulation framework can support tasks ranging from real-time embedded hardware-in-the-loop testing to large-scale Monte Carlo simulation based parametric studies. ROAMS has been successfully used at JPL in several space mission-critical scenarios for NASA across multiple domains (cruise/orbiter, landers, and rovers). ROAMS is unique in its integrated approach to handling the high-fidelity dynamics, sensors, environment, control, and autonomy models that are required for such highly complex missions and are key attributes of future Army unmanned ground vehicles.

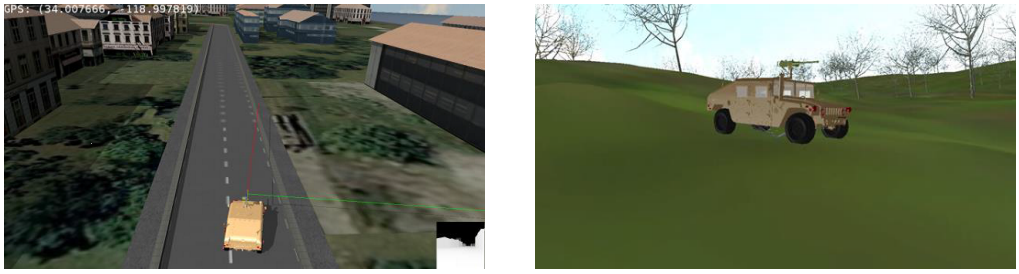

Figure 1: HMMWV UGV simulator: The image on the left depicts an urban driving scenario which exercises the vehicle's autonomous way-point and road following software. The image on the right shows the same vehicle in an off-road scenario with obstacle avoidance capability.

In this project we have adapted the ROAMS vehicle simulation framework to have the following attributes: the model of a common military vehicle (the HMMWV), multibody dynamics based on the fast recursive order-N spatial algebra formulation, wheeled locomotion capability, sensor models (cameras, GPS, radar, LIDAR) and actuators, off-road deformable terrains with vehicle - soil interaction terramechanics models, drive-to-goal locomotion planning with obstacle avoidance, drive/steer to maintain vehicle stability while following a prescribed path and avoiding obstacles, and 3D real-time graphics visualization and data logging capability [3]. The simulator supports both urban and off-road driving scenarios as illustrated in Figure 1.

In this paper we will describe the current status of the UGV simulator - its capabilities, performance benchmarking, validation and evaluation results. The paper also provides an overview and update on current work to enable the

Report Documentation Page

Form Approved
OMB No. 0704-0188

1. REPORT DATE	2. REPORT TYPE	3. DATES COVERED
24 APR 2015		**00-00-2015 to 00-00-2015**

4. TITLE AND SUBTITLE	5a. CONTRACT NUMBER
Advanced Mobility Testbed for Dynamic Semi-Autonomous Unmanned Ground Vehicles	5b. GRANT NUMBER
	5c. PROGRAM ELEMENT NUMBER
6. AUTHOR(S)	5d. PROJECT NUMBER
	5e. TASK NUMBER
	5f. WORK UNIT NUMBER
7. PERFORMING ORGANIZATION NAME(S) AND ADDRESS(ES) **US Army RDECOM-TARDEC,6501 E. 11 Mile Road,Warren,MI,48397-5000**	8. PERFORMING ORGANIZATION REPORT NUMBER
9. SPONSORING/MONITORING AGENCY NAME(S) AND ADDRESS(ES)	10. SPONSOR/MONITOR'S ACRONYM(S)
	11. SPONSOR/MONITOR'S REPORT NUMBER(S)

12. DISTRIBUTION/AVAILABILITY STATEMENT
Approved for public release; distribution unlimited

13. SUPPLEMENTARY NOTES

14. ABSTRACT
See Report

15. SUBJECT TERMS

16. SECURITY CLASSIFICATION OF:			17. LIMITATION OF ABSTRACT	18. NUMBER OF PAGES	19a. NAME OF RESPONSIBLE PERSON
a. REPORT **unclassified**	b. ABSTRACT **unclassified**	c. THIS PAGE **unclassified**	**Same as Report (SAR)**	**11**	

modeling of semi-autonomous vehicle operation which includes integration of the following items: a sophisticated autonomous navigation algorithm with obstacle avoidance, a driver model capable of simulating the input of a human teleoperator, and a shared-control algorithm capable of combining simulated human and autonomous inputs.

2 UGV Autonomy Software

Currently fielded Army unmanned ground vehicles (UGV) are operated remotely by humans who control all actions taken by the UGV. Human teleoperation of UGVs is negatively affected by the effects of latency and reduced situational awareness, while autonomous algorithms still suffer from mission-threatening failure under complex scenarios [4–8]. Because of these drawbacks, the use of shared control methods which blend the strengths of both humans and automation is an area of significant research interest to the Army going forward [9–11]. The Army is interested in using modeling and simulation to enable evaluation of UGV mobility across the full range of shared control options from full teleoperation to full autonomy without having to engage in expensive human testing. New capabilities currently being implemented into ROAMS to model shared control are aimed to keep it at the leading edge of simulation capabilities.

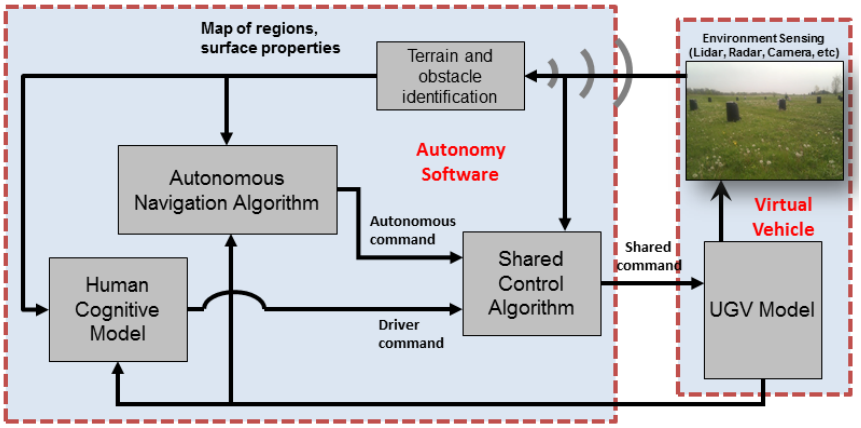

Figure 2: Schematic of the ROAMS simulation of a semi-autonomous UGV adapted from reference [12].

A high-level block diagram of the components necessary for a shared control system is shown in Figure 2. While a long-term goal is to eventually have a suite of models/algorithms to choose from for each of the different components, the current effort involves integration of initial capabilities in each area. This includes the following items: an autonomous navigation algorithm with obstacle avoidance, a driver model capable of simulating the input of a human teleoperator, and a shared-control algorithm capable of combining simulated human and autonomous inputs to model semi-autonomous shared vehicle control.

2.1 Autonomous Navigation Algorithm

The autonomous navigation algorithm being integrated into ROAMS has been developed at the University of Michigan Automotive Research Center (ARC) with TARDEC funding [13]. A block diagram of the algorithm flow is shown in Figure 3. The algorithm uses LIDAR as the obstacle detection sensor, incorporates a multi-stage Model Predictive Control (MPC) formulation, and is specifically designed to be able to handle large vehicles such as a HMMWV operating at high speeds (20-60 mph). It primarily seeks to minimize the travel time to a desired destination location while avoiding obstacles and ensuring vehicle safety, which in practice is defined as avoiding any single wheel liftoff condition. The inherent vehicle dynamic limitations that could lead to wheel lift-off are incorporated into the algorithm in the form of constraints in the optimization formulation which limit the maximum vehicle speed and steering angle control commands generated given the current system state. These constraints are pulled from pre-computed lookup tables produced by a high-fidelity vehicle dynamics model, thus avoiding the need to run such a model in

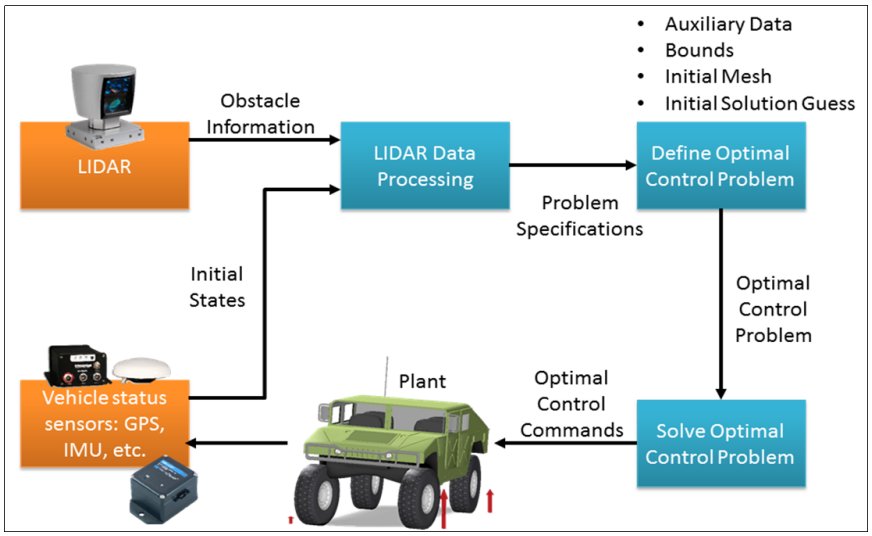

Figure 3: Block diagram of MPC autonomous navigation algorithm from reference [13].

real-time. The algorithm can also incorporate into the optimization known (or estimated) latencies in the vehicle sensing and control actuation systems and mitigate the negative effects of such delays as long as the LIDAR has sufficient range.

2.2 Driver Model

The driver model being integrated is a modified version of a highway driver model developed at Drexel University and implemented in the ACT-R cognitive architecture [14]. ACT-R (short for Adaptive Control of Thought-Rational) is a high level model of human cognition embedded into a computational framework [15]. The driver model is a specialized task model written in the ACT-R language which simulates the sensory/motor performance of a human driver. At present the driver model can simulate a teleoperator trying to follow a predefined path under different latency conditions. It produces steering and throttle control inputs that can be directly applied to the vehicle model. Adding an interface to the general ACT-R architecture into ROAMS as is being done in the current project will allow new cognitive task models to be added in the future which can simulate other aspects of operator performance.

2.3 Shared Control Algorithm

The shared control algorithm being integrated was developed at MIT and performs a proportional blending of the control inputs provided by the autonomous algorithm and the human driver model [12]. A blending value k is computed by the algorithm with $\mathrm{k} = 0$ representing pure teleoperation where only the operator control input is applied and $\mathrm{k} = 1$ representing pure autonomous operation. The exact value of k used depends on the computation of a threat metric which is meant to represent how close the system is to a mission ending failure (such as vehicle rollover). As the computed threat increases, so does the value of k, but the exact nature of the $\mathrm{k}(\mathrm{threat})$ function is configurable. It can be based on one or more system state variables and can vary from a simple linear relationship to more complicated monotonically increasing functions depending on desired performance considerations.

3 UGV Dynamics Model

An emphasis of this research is to achieve close to real-time dynamics performance for allowing the closed-loop testing of unmanned ground vehicles (UGV) for urban as well as off-road scenarios. The overall vehicle simulator performance is governed by the multibody dynamics model for the vehicle, the wheel/terrain interaction dynamics

and the sensor models. Our modeling approach is tailored to support accurate dynamics model for ground vehicles with complex suspension dynamics while meeting the computational performance goals.

The simulator's architecture allows the seamless selection of different fidelity levels and model parameters across the full modeling suite, and more importantly, provides analysts with a modular way to swap component models for changing vehicle/control/sensor behavior. A critical aspect of our UGV simulator is its use of the recently developed constraint embedding technique for modeling the dynamics of the HMMWV suspension system which consists of a double wishbone suspension at each wheel of the vehicle. Not only does the constraint embedding approach reduce the size of the dynamics model, but it also leads to an over 100x speed up over conventional dynamics modeling methods as measured in benchmark tests.

The UGV simulation architecture represents a shift in paradigm by empowering analysts with full visibility and control in tailoring key elements of the simulator. This scalable architecture allows the adaptation and tuning of simulation fidelity across a very broad range (e.g. rigid/flex-body dynamics, sensor fidelity, dynamics/kinematics modes) needed for the multi-layered testing of complex autonomy behaviors. The modular design also allows the insertion and closing the loop with vehicle autonomy modules and sensor packages for the evaluation of system level performance and carrying out trade studies to optimize design metrics without sacrificing essential fidelity characteristics. This feature is in contrast with alternative approaches that provide narrow capabilities for specialized aspects such as sensor fidelity, vehicle dynamics, or behavioral models that address only a narrow slice of vehicle autonomy simulation needs. This simulation approach has been successfully used by analysts across multiple NASA centers for a variety of problems.

The details of the vehicle dynamics and sensor modeling have been described in reference [3] and we provide a brief overview here. We describe in more detail our recent work in extending the tire/soil interaction models to include hard/soft tire and terrain model dynamics within the UGV simulator.

3.1 Vehicle Modeling

We describe here the multibody dynamics modeling approach for our reference 4-wheeled vehicle, which has a double wishbone suspension and associated spring-damper unit at each wheel (Figure 4). Each of these wheel suspensions contains a number of articulated bodies with multiple kinematic closed loops. Due to the constraints, each suspension has only a single effective degree of freedom.

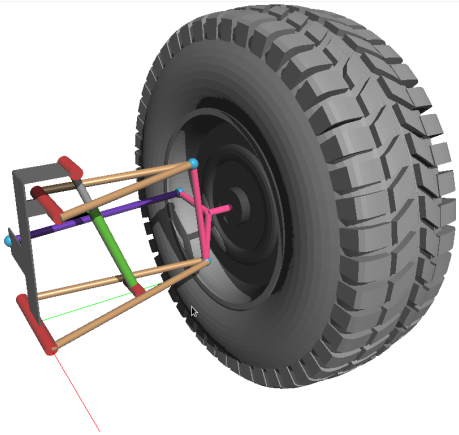

Figure 4: The double wishbone suspension for a single wheel.

The standard approach for modeling closed-chain system dynamics [16] decomposes the system into a a set of independent bodies, and appends the closed-chain bilateral constraints to the equations of motion. A drawback of this absolute coordinates approach (also referred to as the *fully augmented (FA)* approach) is the high computational cost for solving the equations of motion. Another serious drawback is the constraint violation error drift that arises during the integration of the multibody dynamics equations of motion. This error drift is usually handled by the use of a differential-algebraic equation (DAE) solver and error correction algorithms to manage the constraint error over time, adding even more computational cost and accuracy error to the dynamics solution. Our real-time performance needs require us to find alternative solutions to overcome these major computational drawbacks of the conventional approach.

Instead of the absolute coordinates dynamics formulation, we use a minimal coordinates approach for the dynamics modeling. One advantage of the minimal coordinates approach is that the size of the dynamics model is significantly smaller. Moreover, the minimal coordinates model allows us to use structure-based low-cost recursive dynamics algorithms [17] whose computational cost scales only linearly with the number of degrees of freedom.

An area that required special attention was the handling of the closed-loop constraints within the wheel suspensions which are not supported by the recursive dynamics algorithms. For this, we turned to the recently developed *constrained embedding (CE)* techniques developed using the *spatial operator algebra (SOA)* methodology [17, 18].

The constraint embedding technique uses graph transformation techniques to convert the multibody systems with graph topologies into ones with tree topology, and thereby once again allowing the direct use of the O(N) recursive algorithms for solving the system dynamics. The CE graph transformation process converts all constraint loops into variable configuration compound bodies which have the same number of degrees of freedom as the number of independent degrees of freedom for the loops they replace. These compound bodies locally handle their internal degrees of freedom and constraint, effectively hiding them from the dynamics solver. Thus the resulting system topology is once again a tree with only inter-body hinges and no bilateral constraints.

Besides allowing the use of the recursive O(N) tree algorithms, this formulation allows the use of simpler ODE integrators instead of DAE integrators. Moreover no additional error control techniques are needed. The SOA methods allow us to simplify and implement CE algorithms and handle the aggregated bodies with configuration dependent geometry. While the CE method shares the minimal coordinates attribute with projection dynamics techniques [16, 19], its advantage lies in the preservation of the system's tree topology structure that is necessary for the use of the structure-based recursive algorithms. The CE approach for the multibody modeling of the vehicle and suspension dynamics is described in detail in reference [20]. Table 3.1 (from reference [3]) summarizes the speed comparison between the FA and CE vehicle dynamics solution methods. Also included in the table is the *tree augmented (TA)* method which also exploits recursive minimal coordinate techniques but still has to work with explicit closed-loop constraints. The FA dynamics model is over 14 times larger and 120 times slower than the CE model.

Method	Number of degrees of freedom	Number of constraints	Overall size	Simulation time ratio
CE	15	0	15	1
TA	45	30	75	4.1
FA	216	201	417	120.0

Table 1: A comparison of the dynamics model size and computational speed for the FA, TA and CE formulations for the HMMWV vehicle.

The use of advanced dynamics techniques such as CE have been critical to achieving the simulation performance needed for our UGV testbed. To the best of our knowledge, this is the first instance of the application of these new techniques for modeling complex vehicle system dynamics without sacrificing dynamics fidelity. We have made considerable improvements recently to increase the CE algorithm speed even further, and the updated benchmark performance results can be found in reference [20].

3.2 Modeling rigid wheel on soft soil

We are using the Bekker approach for modeling the dynamics model of a rigid wheel interacting with soft soil [21–23] and provide a brief overview of the model here. Bekker's relationship between static sinkage and normal stress is

$$\sigma(h) = \left(\frac{k_c}{b} + k_\phi\right) h^n \tag{1}$$

where b denotes the wheel width. The entry and exit angles (Figure 5) are related to the total sinkage and exit penetration as follows

$$\theta_f = \arccos(1 - h/R_{ul}) \quad \text{and} \quad \theta_r \quad = \arccos(1 - h_e/R_{ul}) \tag{2}$$

The exit penetration h_r depends on the elastic stiffness K_s of the soil. The *angle of maximum stress* θ_m is

$$\theta_m = (a_0 + a_1 S_L)\theta_f \tag{3}$$

The *wheel normal normal stress distribution* $\sigma(\theta)$ is

$$\sigma(\theta) = \begin{cases} \left(\frac{k_c}{b} + k_\phi\right)\left(R_{ul}\left(\cos(\theta) - \cos(\theta_f)\right)\right)^n & \text{for } \theta_m \leqslant \theta < \theta_f \\ \left(\frac{k_c}{b} + k_\phi\right)\left(R_{ul}\left(\cos\left(\theta_f - \frac{(\theta-\theta_r)}{(\theta_m-\theta_r)}(\theta_f - \theta_m)\right) - \cos(\theta_f)\right)\right)^n & \text{for } \theta_r \leqslant \theta < \theta_m \end{cases} \tag{4}$$

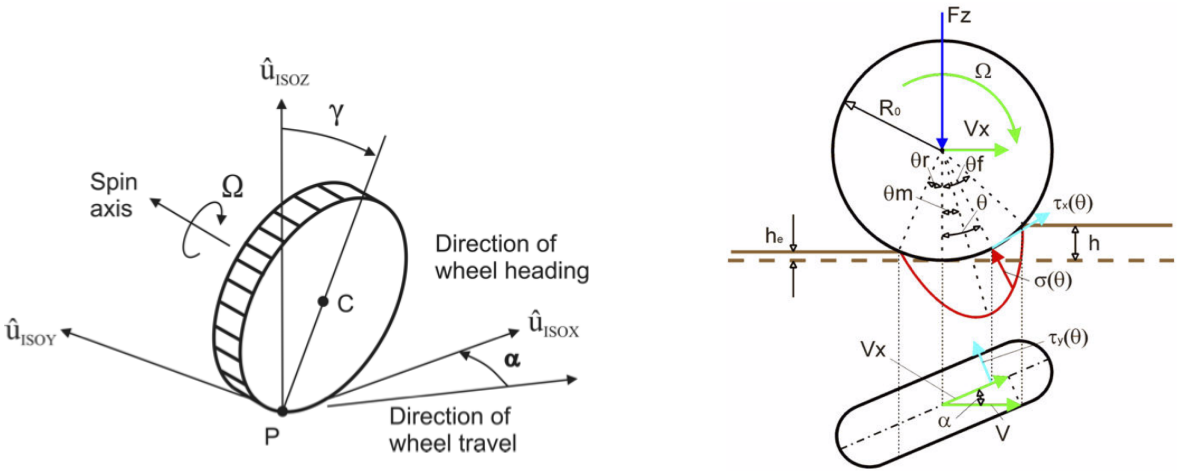

Figure 5: Figures showing the geometry of wheel sinkage (left) and stress distribution under the wheel (right) from reference [24].

With $\tau_{max}(\theta) = c + \sigma(\theta)\tan(\phi)$. the *shear stresses* in the longitudinal direction $\tau_x(\theta)$ and the lateral direction $\tau_y(\theta)$ are

$$\tau_x(\theta) = \tau_{max}(\theta)\left(1 - \exp^{-\frac{|j_x(\theta)|}{k_x}}\right) \quad \text{and} \quad \tau_y(\theta) = \tau_{max}(\theta)\left(1 - \exp^{-\frac{|j_y(\theta)|}{k_y}}\right) \tag{5}$$

where the *longitudinal* and *lateral shear displacements* $j_x(\theta)$ and $j_y(\theta)$ respectively are [23]

$$j_x(\theta) = R_{ul}(\theta_f - \theta) - \frac{v_x}{\Omega}(\sin(\theta_f) - \sin(\theta) \quad \text{and} \quad j_y(\theta) = \frac{v_y}{\Omega}(\theta_f - \theta) \tag{6}$$

and the *longitudinal* and *lateral shear modulus* k_x and k_y respectively are

$$k_x = k_{x0} + k_{x1}\alpha, \qquad k_y = k_{y0} + k_{y1}\alpha \tag{7}$$

The components of the force vector $f(\theta) = [f_x, f_y, f_z]^*$ are given by

$$\begin{aligned} f_x(\theta) &= R_{ul}(\tau_x(\theta)\cos(\theta) - \sigma(\theta)\sin(\theta)) && \text{(longitudinal force)} \\ f_y(\theta) &= R_{ul}\tau_y(\theta) && \text{(lateral force)} \\ f_z(\theta) &= R_{ul}(\tau_x(\theta)\sin(\theta) + \sigma(\theta)\cos(\theta)) && \text{(vertical load)} \end{aligned} \tag{8}$$

The overall force F and moment M at the wheel center are

$$F = b\int_{\theta_r}^{\theta_f} f(\theta)d\theta, \qquad M = b\int_{\theta_r}^{\theta_f} (R(\theta) \times f(\theta))d\theta \tag{9}$$

The components of M are referred to as the *overturning moment*, the *rolling resistance moment* and the *aligning moment*.

3.3 Modeling soft tire on rigid terrain

This section presents the Fiala model for modeling the dynamics interaction of a deformable soft tire with rigid terrain such as paved roads. The Fiala tire model, developed by Fiala in 1954 is a simplified model that does not require extensive and complicated physical tests to determine the necessary parameters.

The *normal force* F_z, as shown in Figure 6 is:

$$F_z = \max((k_t\delta + c_t\dot{\delta}), 0) \tag{10}$$

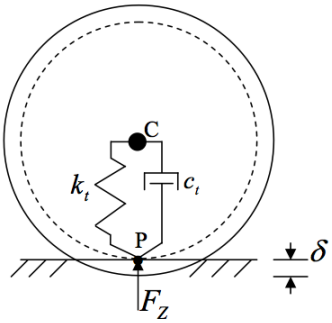

Figure 6: The figure on the left illustrates the tire normal force computation model, and the one of the left key wheel kinematic parameters from reference [25].

The maximum function ensures that the normal force is zero when the tire is not in contact with the ground.

Given the longitudinal speed v_x, the tire loaded radius R_l, and the tire angular speed Ω, also shown in Figure 6, the tire *longitudinal deflection (slip)* S_L is [26, 27]:

$$S_L = \begin{cases} 1 - \frac{v_x}{R_l \Omega} = 1 - \frac{R_e}{R_l} & \text{for } v_x < R_l\Omega \text{ (driving) or } R_e < R_l \\ \frac{R_l \Omega}{v_x} - 1 = \frac{R_l}{R_e} - 1 & \text{for } v_x > R_l\Omega \text{ (braking) or } R_e > R_l \end{cases} \tag{11}$$

Slip value of 0 implies no slippage. The limiting value of 1 corresponds to zero longitudinal velocity with non-zero angular velocity (i.e. spinning in place), while the limiting value of -1 corresponds to zero angular velocity with non-zero longitudinal velocity (i.e. pure sliding).

The *transversal deflection* α or *lateral slip angle* and the *lateral slip coefficient* S_α are

$$S_\alpha = \tan(\alpha) = \frac{-v_y}{v_x} \tag{12}$$

The *comprehensive slip ratio* $S_{L\alpha}$

$$S_{L\alpha} = \sqrt{S_L^2 + S_\alpha^2} \tag{13}$$

The instantaneous value of the *coefficient of friction* μ is obtained by linear interpolation between μ_0 and μ_1 using $S_{L\alpha}$ as follows:

$$\mu = \mu_0 - S_{L\alpha}(\mu_0 - \mu_1) \tag{14}$$

The *critical value of longitudinal slip ratio* S_L^* below which the tire is in elastic deformation state, and beyond which the tire is in full longitudinal sliding:

$$S_L^* = \left| \frac{\mu F_z}{2 C_S} \right| \tag{15}$$

The *critical value of lateral slip angle* α^* below which the tire is in elastic deformation state, and beyond which the tire is in full lateral sliding state:

$$S_\alpha^* = \tan(\alpha^*) = \left| \frac{3\mu F_z}{C_\alpha} \right| \tag{16}$$

The *slip angle intermediate parameter* H which is negative during full lateral slippage and non-negative otherwise:

$$H = 1 - \frac{C_\alpha |S_\alpha|}{3\mu |F_z|} = 1 - \left| \frac{S_\alpha}{S_\alpha^*} \right| \tag{17}$$

The force and moment expressions for the Fiala tire model [28] are as follows. The longitudinal force (or drawbar pull) is:

$$F_x = -\begin{cases} C_S S_L & \text{for } |S_L| < S_L^* \text{ (elastic deformation)} \\ \operatorname{sgn}(S_L)\left(\mu F_z - \frac{(\mu F_z)^2}{4|S_L| C_S}\right) & \text{for } |S_L| \geqslant S_L^* \text{ (full longitudinal slip)} \end{cases} \tag{18}$$

The transverse force is:

$$F_y = \text{sgn}(\alpha) \begin{cases} -\mu |F_z|(1 - H^3) & \text{for } |\alpha| < \alpha^* \text{ (elastic deformation)} \\ -\mu |F_z| & \text{for } |\alpha| \geqslant \alpha^* \text{ (full lateral slip)} \end{cases} \tag{19}$$

The overturning moment is $M_x = 0$. The lateral moment is

$$M_y = \begin{cases} -C_r F_z & \text{for } \Omega < 0 \text{ (rolling forwards)} \\ C_r F_z & \text{for } \Omega >= 0 \text{ (rolling backwards)} \end{cases} \tag{20}$$

Finally, the normal (aligning) moment is:

$$M_z = \begin{cases} 2R_2 \mu |F_z|(1 - H) H^3 \,\text{sgn}(\alpha) & \text{for } |\alpha| < \alpha^* \text{ (elastic deformation)} \\ 0 & \text{for } |\alpha| \geqslant \alpha^* \text{ (full lateral slip)} \end{cases} \tag{21}$$

This takes into account the effect of the pneumatic trail.

3.4 Modeling soft tire on soft soil

As illustrated in Figure 7, a tire on soft soil incurs tire deformation as well as sinkage. We use the *surrogate circle* approach [24, 29–33] to better approximate the tire contact surface with the ground. The surrogate circle is assumed to pass through the entry and exit points of contact with the terrain, and furthermore be tangential to the ground at the exit point. The relationship of the surrogate circle radius R_s to the R_{ul}, the tire deformation δ and sinkage h can be obtained using the following series of chord/radius expressions from Figure 7:

$$\begin{aligned} X^2 &= \delta(2R_{ul} - \delta) \\ Y^2 &= (\delta + h)(2R_{ul} - \delta - h) \\ (X + Y)^2 &= h(2R_s - h) \\ \Rightarrow \sqrt{h(2R_s - h)} &= \sqrt{\delta(2R_{ul} - \delta)} + \sqrt{(\delta + h)(2R_{ul} - \delta - h)} \end{aligned} \tag{22}$$

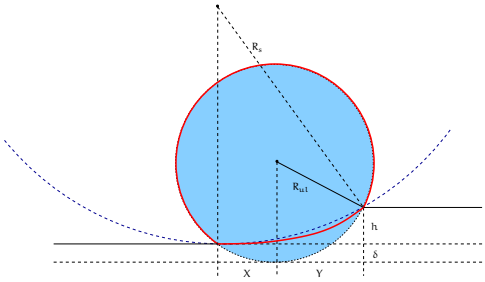

Figure 7: Surrogate circle for tire on soft soil.

Assuming that $R_s, R_{ul} \gg \delta, h$, the above reduces to the following simpler approximate relationship [30]

$$\sqrt{\frac{R_s}{R_{ul}}} \approx \sqrt{1 + \frac{\delta}{h}} + \sqrt{\frac{\delta}{h}} \tag{23}$$

The surrogate circle radius R_s is used in the Bekker model to compute the forces and moments on the wheel. To determine the δ and h values, The condition that the normal load F_z from the Bekker model (using the surrogate circle radius) Eq. 9 should equal the normal load from the tire deformation Eq. 10. Thus, given $\delta + h$ from the system kinematic state, the tire deflection δ and soil sinkage h values are determined iteratively subject to satisfying the normal loads equality and the supporting circle radius expression in Eq. 23.

4 Results

The results to date show that the ROAMS HMMWV simulator can model high fidelity multibody dynamics, terrain, sensors, actuators, control and navigation algorithms in urban and off-road scenarios at speeds that are beneficial for autonomous UGV analysis and design purposes.

As an example, a simulation of a HMMWV in a NATO double lane-change (DLC) scenario was run using both ROAMS and MSC ADAMS, a industry standard high-fidelity modeling and simulation environment. Figure 8 and 9 show the vehicle paths simulated in the two environments and comparisons of the computed values for various dynamics parameters. The two paths are not exactly identical, therefore the dynamics results should not be exact matches but the results represent a good match in a qualitative sense as well as in computed parameter magnitude as shown in Figure 10.

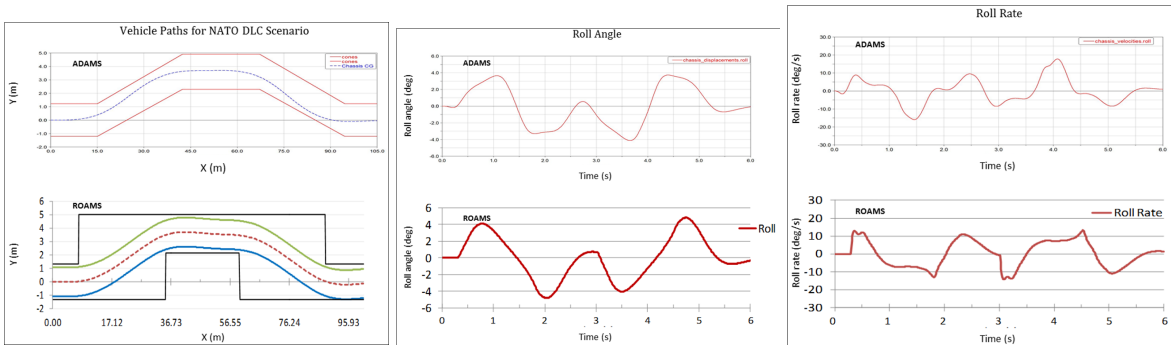

Figure 8: Vehicle paths for double lane change maneuver, and the roll angles and rates from the ADAMS and ROAMS simulations.

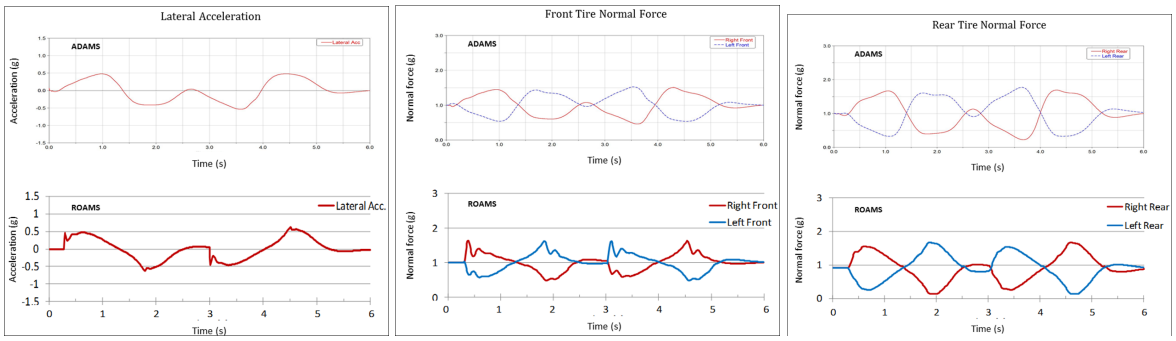

Figure 9: Comparison of the vehicle lateral acceleration, and the front and rear tire normal forces from the ADAMS and ROAMS simulations.

The ROAMS and ADAMS results were generated on a single core of an Intel Core I7-2600 CPU at 3.4 GHz. Even without significant attempts to optimize performance, Table 10 shows that ROAMS on a single core ran at 3.4x real-time and was 2.5x faster than ADAMS with comparable dynamic fidelity. The ROAMS simulator included vehicle dynamics as well as simulations of sensors such as cameras, lidar and GPS units while ADAMS simulated only the vehicle dynamics. This demonstrates that the closed-loop performance evaluation and testing of onboard UGV autonomy for the U.S. Army vehicles can be carried out in simulation by ROAMS without having to sacrifice crucial vehicle dynamics fidelity for the sake of performance speed. The performance of ROAMS will continue to be improved based on further optimization.

Response		ADAMS Max	ADAMS Min	ROAMS Max	ROAMS Min
Tire Vertical Forces (g)	Left Front	1.5	0.5	1.6	0.5
	Right Front	1.5	0.5	1.6	0.5
	Left Rear	1.8	0.3	1.7	0.1
	Right Rear	1.7	0.2	1.7	0.1
Lateral Acceleration (g)		0.5	-0.5	0.6	-0.6
Body Roll Angle (deg)		4.1	-3.7	4.8	-4.8
Body Roll Rate (deg/s)		16.0	-17.8	13.2	-14.4
CPU Time per Simulation Time (s/s)		8.8[a]		3.4[b]	

Figure 10: Simulation comparison.

5 Conclusions

This paper provides an overview of the ROAMS UGV simulator and an update on current work to add new capabilities to the software. These new capabilities include improved terramechanics models as well as algorithms for modeling semi-autonomous control of UGVs. These enhancements will allow ROAMS to help meet the Army's UGV modeling and simulation needs. Testing and evaluation have shown that ROAMS can provide closed-loop simulation of UGV systems for the Army without having to sacrifice crucial vehicle dynamics fidelity for the sake of performance speed.

Acknowledgments

The research described in this paper was performed at the U.S. Army TARDEC, and at the Jet Propulsion Laboratory (JPL), California Institute of Technology, under contract with the National Aeronautics and Space Administration.[1]

References

[1] P. Jayakumar, W. Smith, and B. A. Ross, "Development of High Fidelity Mobility Simulation of an Autonomous Vehicle in an Off-road Scenario Using Integrated Sensor, Controller, and Multi-Body Dynamics," in 2011 NDIA Ground Vehicle Systems Engineering and Technology Symposium, Dearborn, MI, 2011.

[2] A. Jain, J. Guineau, C. Lim, W. Lincoln, M. Pomerantz, G. Sohl, and R. Steele, "Roams: Planetary Surface Rover Simulation Environment," in International Symposium on Artificial Intelligence, Robotics and Automation in Space (i-SAIRAS 2003), Nara, Japan, May 2003.

[3] J. M. Cameron, S. Myint, C. Kuo, A. Jain, H. Grip, P. Jayakumar, and J. Overholt, "Real-Time and High-Fidelity Simulation Environment for Autonomous Ground Vehicle Dynamics," in 2013 NDIA Ground Vehicle Systems Engineering and Technology Symposium, Troy, Michigan, 2013.

[4] J. Y. Chen, E. C. Haas, and M. J. Barnes, "Human performance issues and user interface design for teleoperated robots." Ieee Transactions On Systems Man And Cybernetics, vol. 37, no. 6, pp. 1231–1245, 2007.

[5] L. Gomes, "Hidden Obstacles for Google's Self-Driving Cars," MIT Technology Review, 2014.

[6] U. Ozguner, C. Stiller, and K. Redmill, "Systems for safety and autonomous behavior in cars: The DARPA Grand Challenge experience," Proceedings of the IEEE, vol. 95, no. 2, pp. 397–412, 2007.

[7] M. Campbell, M. Egerstedt, J. P. How, and R. M. Murray, "Autonomous driving in urban environments: approaches, lessons and challenges," Philosophical Transactions of the Royal Society A: Mathematical, Physical and Engineering Sciences, vol. 368, no. 1928, pp. 4649–4672, 2010.

[8] J. P. Gray, R. E. Karlsen, C. DiBerardino, E. Mottern, and N. J. Kott, "Challenges to autonomous navigation in complex urban terrain," in SPIE Defense, Security, and Sensing (pp. 83870B-83870B). International Society for Optics and Photonics, 2012.

[9] R. Parasuraman, T. B. Sheridan, and C. D. Wickens, "A model for types and levels of human interaction with automation," IEEE Transactions on Systems, Man and Cybernetics, vol. 30, no. 3, pp. 286–297, 2000.

[10] F. Flemisch, M. Heesen, T. Hesse, J. Kelsch, A. Schieben, and J. Beller, "Towards a dynamic balance between humans and automation: authority, ability, responsibility and control in shared and cooperative control situations," Cognition, Technology & Work, vol. 14, no. 1, pp. 3–18, 2012.

[11] C. A. Miller and R. Parasuraman, "Designing for flexible interaction between humans and automation: Delegation interfaces for supervisory control," Human Factors: The Journal of the Human Factors and Ergonomics Society, vol. 49, no. 1, pp. 57–75, 2007.

[12] S. J. Anderson, S. C. Peters, T. E. Pilutti, and K. D. Iagnemma, "An optimal-control-based framework for trajectory planning, threat assessment, and semi-autonomous control of passenger vehicles in hazard avoidance scenarios," International Journal of Vehicle Autonomous Systems, vol. 8, no. 2/3/4, p. 190, 2010.

[13] J. Liu, J. L. Stein, P. Jayakumar, and T. Ersal, "A Multi-Stage Optimization Formulation for MPC-Base Obstacle Avoidance in Autonomous Vehicles using Lidar Sensor," in Proceedings of the ASME 2014 Dynamic Systems and Control Conference, San Antonio, TX, 2014, pp. 1–10.

[14] D. D. Salvucci, "Modeling driver behavior in a cognitive architecture," Human Factors: The Journal of the Human Factors and Ergonomics Society, vol. 48, no. 2, pp. 362–380, 2006.

[15] J. R. Anderson, "An integrated theory of the mind," Psychological review, vol. 111, no. 4, p. 1036, 2004.

[16] E. J. Haug, Elements of Computer-Aided Kinematics and Dynamics of Mechanical Systems: Basic Methods. Springer-Verlag, 1984.

[17] A. Jain, Robot and Multibody Dynamics: Analysis and Algorithms. Springer, 2011.

[18] ——, "Multibody graph transformations and analysis Part II: Closed-chain constraint embedding," Nonlinear Dynamics, vol. 67, no. 3, pp. 2153–2170, Aug. 2012.

[19] R. von Schwerin, Multibody system simulation: numerical methods, algorithms, and software. Springer, 1999.

[20] A. Jain, C. Kuo, P. Jayakumar, and J. M. Cameron, "A Constraint Embedding Approach for Complex Vehicle Suspension Dynamics," in Multibody Dynamics 2015, ECCOMAS Thematic Conference, Barcelona, Spain, 2015.

[21] G. Ishigami, K. Nagatani, A. Miwa, and K. Yoshida, "Terramechanics-based Model for Steering Maneuver of Planetary Exploration Rovers on Loose Soil," Journal of Field Robotics, vol. 24, no. 3, pp. 233–250, 2007.

[22] Z. Jia, W. Smith, and H. Peng, "Fast Analytical Models of Wheeled Locomotion in Deformable Terrain for Mobile Robots," Robotica, vol. 35, no. 35-53, 2013.

[23] F. Zhou, R. E. Arvidson, K. Bennett, B. Trease, R. Lindemann, P. Bellutta, K. D. Iagnemma, and C. Senatore, "Simulations of Mars Rover Traverses," Journal of Field Robotics, vol. 31, no. 1, pp. 141–160, Jan. 2014.

[24] "ADAMS/Tire model documentation," 2014.

[25] W. Bombardier, "Symbolic Modelling and Simulation of Wheeled Vehicle Systems on Three-Dimensional Roads," Ph.D. dissertation, University of Waterloo, 2009.

[26] J. Y. Wong, Theory of Ground Vehicles, 3rd ed. New York, New York, USA: John Wiley & Sons, 2001.

[27] E. Bakker, L. Nyborg, and H. B. Pacejka, "Tyre Modelling for Use in Vehicle Dynamics Studies (paper no. 870421)," SAE Technical Paper, Tech. Rep., 1987.

[28] M. Blundell and D. Harty, The Multibody Systems Approach to Vehicle Dynamics. Warrendale, Pennsylvania: Society of Automotive Engineers, Inc, 2004.

[29] M. G. Bekker, Introduction to terrain-vehicle systems. Ann Arbor: The University of Michigan Press, 1969.

[30] I. C. Schmid, "Interaction of vehicle and terrain results from 10 years research at IKK," Journal of Terramechanics, vol. 32, no. 1, pp. 3–26, 1995.

[31] "RecurDyn Tire model documentation," 2014.

[32] "AS2TM Tire Model User's Guide," 2015.

[33] H. Li, "Analysis of Off-Road Tire-Soil Interaction through Analytical and Finite Element Methods," Ph.D. dissertation, University of Kaiserslautern, 2013.